Seasonal morphological response of an open sandy beach to winter wave conditions: The example of Biscarrosse beach, SW France

Mélanie Biausque, Nadia Senechal

Version of Record: https://www.sciencedirect.com/science/article/pii/S0169555X19300431
Manuscript_751283f14410b4489d737c340fc4e382

Seasonal morphological response of an open sandy beach to winter wave conditions: the example of Biscarrosse beach, SW France.

Mélanie BIAUSQUE [a*], Nadia SENECHAL [b]

a. Université de Bordeaux, OASU, UMR CNRS 5805 EPOC – OASU,

Allée Geoffroy Saint-Hilaire, CS 50023, 33615 Pessac cedex, France.

*Corresponding author: melanie.biausque@u-bordeaux.fr

b. Université de Bordeaux, OASU, UMR CNRS 5805 EPOC – OASU,

Allée Geoffroy Saint-Hilaire, CS 50023, 33615 Pessac cedex, France.

nadia.senechal@u-bordeaux.fr

Abstract

18 months of at least bi-weekly topographic surveys have been conducted on a 700 m stretch of the meso- to macro-tidal Biscarrosse beach, France. Here we focus on the impact of the short-term dynamics of the beach (a few days) on the seasonal winter response of the beach. The beach was surveyed intensively during two winter seasons and the results indicate that despite similar pre-winter morphology but very contrasting energy levels (the first winter season being 1.7 times more energetic than the second winter season), the sediment budgets over the two winter periods were very similar as well as the cross-shore dynamics of the extracted proxies associated with the dune foot and the berm. The data collected suggest that this may be explained by the sequence of erosion/recovery events driven by hydrodynamic conditions (as the water level and energetic conditions), and sediment transport. Thus, during the first winter, post-storm recovery was effectively driven by energetic conditions while during the second winter, inter-storm conditions did not allow the initiation of recovery in between the storms. Apart from the control from wave

conditions, the seasonal beach response is also discussed within the framework of storm chronology and tidal range.

Keywords: Sandy beach morphology, Sediment budget, Shoreline proxies, Short-term dynamics

Introduction

Approximately 31% of the world coastline is represented by sandy coasts and 24% of the sandy shoreline extracted from satellite images is classed as eroding (Luijendijk et al., 2018). Scientifically complex and economically attractive, sandy shores evolve at different timescales, from hours (tide or event scales) to decades (Stive et al., 2002). They are also commonly recognized as the last natural buffer against flooding (e.g. Anthony, 2013). In the context of a changing climate, the elevation of water levels associated with changing hydrodynamic conditions, both through sea-level rise and an increase in extreme storms, threaten sandy shores and coastal infrastructure (e.g. Marshall et al., 2001; Feagin et al., 2005; Stive et al., 2013). Forecasting the evolution of sandy shores has been a challenging task for many decades.

Wright & Short (1984) proposed a classification of the morphology of sandy beaches based on the concept of morphodynamic adjustment between the beach and the environmental forcing (predominantly waves). In this classification the beach can evolve from a dissipative state, associated with energetic waves and characterized by a relatively uniform morphology and the absence of a berm, to a reflective state associated with low energetic conditions and characterized by the presence of a berm. In between, four intermediate states are described and distinguished by the alongshore variability. This classification also relies on the cross-shore sediment transfers between the lower and the upper beach: energetic periods being associated with offshore sediment transport (erosion) and calm conditions with onshore sediment transport (accretion). This concept has been further extended in Masselink & Pattiaratchi (2001), who resumed the “cycle of beach” (previously exposed by Wright & Short, 1984) as depending on the wave energy level: energetic wave conditions induce beach erosion and a sandbar formation, while accretion of the beach and a berm development are observable under calmer conditions. In temperate environments where wave climate typically shows distinct seasonality, two types of cycles can be defined: a seasonal cycle based on the winter/summer morphological changes, and an event cycle that follows the

storm/post-storm evolutions of the systems. In these environments it is thus acknowledged that beaches will essentially undergo erosion during the winter season and then recover during the summer period (e.g. Larson & Kraus, 1989; Yates et al., 2009; Splinter et al., 2013). However, wave dominated sandy beaches are submitted to multiple physical processes and the morphological response to the forcing is non-linear (Castelle et al., 2007; Masselink & van Heteren, 2014; Masselink et al., 2016). There remains a need to better understand these dynamics, specifically how short-term event-scale dynamics can modify the medium-term seasonal response. Over the past years much attention has been paid to the impact of storms in terms of erosion with the development of models as Xbeach, which shows reasonable skill in simulating short-term seasonal erosion (Dissanayake et al., 2015; Davidson et al., 2017). Nevertheless, there remains a knowledge gap in the data-driven understanding of the beach evolution between consecutive storm events and during the seasonal recovery of the system (e.g. Scott et al., 2016; Harley et al., 2017; Splinter et al., 2018).

In the field, two approaches have been generally adopted to better study beach morphodynamics: a long-term approach to access seasonal, annual to decadal beach evolution and recovery from dramatic events (van Rijn, 2009; Corbella & Stretch, 2011; Pender and Karunarathna, 2013; Scott et al., 2016) and a short-term approach focusing on the event temporal scale (e.g. Coco et al., 2014; Ludka et al., 2015; Harley et al., 2017). Long-term approaches rely generally on long-term data set but with a poor temporal resolution while short-term approaches often only cover a few weeks but with a high temporal resolution. Video imagery can bridge the gap (e.g. Lippmann & Holman, 1989; Aarninkhof et al., 2003; Smith & Bryan, 2007; Senechal et al., 2015; Biausque et al., 2016; Angnuureng et al., 2017), but the uncertainties associated with the extracted proxies make it challenging to use them under specific conditions.

Another bias often impacting long-term data sets, is that generally only one proxy is measured which may influence the interpretations of the results (e.g. Boak & Turner, 2005). Thus, long-term beach morphodynamic studies are often based on a single proxy that is qualified as representative of the

shoreline: for example, the dune foot (e.g. Battiau-Queney et al., 2003), the limit of the wet and dry sand (e.g. van de Lageweg et al., 2013) or a single isocontours (e.g. Senechal et al, 2009; Angnuureeng et al., 2017).

The aim of this work is to improve our understanding of the impact of short-term variability on the seasonal response of the beach by presenting a new and original data set. The originality of this work is to use a detailedmorphological long-term data set (covering 16 months) collected at high frequency (at least 2/weeks during winter seasons) on an open sandy beach dominated by the wave energy. In particular two winter seasons with contrasting hydrodynamic conditions but similar morphological response were surveyed and the data set allowed investigation of both dynamics at the seasonal scale (several months) and the recovery and erosion periods at event scale (a few days) within each winter season. The considerable number of surveys constituting this exceptional database also offers the possibility to extract and compare different proxies and to calculate sediment budget at both the seasonal and event scales. Thus, the sediment budget of different sections of the beach profile (dune, berm, lower intertidal beach) are investigated. In the next section, methods and data are presented. Then results allow discussions about the impact of short scale response of the beach on the winter seasonal response of the system.

Methods and data

1. Study site

Biscarrosse beach, one of the field sites of the French National Network for shoreline observations (SNO Dynalit), is located on the South French Atlantic coast (Fig.1A). This site is characterized by a double-barred meso- to macrotidal open sandy beach, with tidal range values about 3.2 m on average that can reach 5 m during spring tides (Castelle et al., 2007), backed by a relatively high dune

(17-18 m high, Almar et al., 2009). With an orientation about 10.5° from the north, Biscarrosse is dominated by the North Atlantic swell, with mean annual significant wave height (H_s) of 1.4 m and annual averaged mean periods (T_{mean}) of 6.5 s (Butel et al., 2002). The wave climate on the Aquitanian coast is characterized by a strong seasonality; the annual and seasonal statistics were precisely described by Butel et al. (2002). They summarized that during winter seasons (for November to March) the $H_{s(winter)}$ is approximately 2 m with $H_{s(Storms)}$ that can exceed 10m while in summers H_s can be less than 0.5 m.

The beach is composed of median grain size sand (D_{50} = 350 µm) and generally exhibits a double sand bar system (Ba & Senechal, 2013; fig.1D). Following the classification proposed by Wright & Short (1984) Biscarrosse can be classified as an intermediate beach associated with an inner bar that exhibits Transverse Bar and Rip (TBR) and Low Tide Terrace (LTT) morphology (Peron & Senechal, 2011). However, all intermediate states can be observed. The outer bar morphology is typically crescentic associated with a wavelength of approximately 700 m (Lafon et al., 2004; Castelle et al., 2007b). Short-term morphological changes (typically < 1 year) are essentially led by cross-shore exchanges but at multi-annual scale the north to south directed significant longshore drift (e.g. Abadie et al., 2006; Idier et al., 2013) may also influence the area (Dehouck et al., 2012). Using 6 years of daily video extracted shoreline proxies, Angnuureng et al. (2017) showed that the shoreline variability at Biscarrosse is mainly driven by seasonal variations (52%) and short term events (28%).

Biscarrosse cannot be considered as a fully natural system, as diverse management strategies are deployed along the beach-dune system. The back dune is covered by grass in order to be accessible and more attractive to tourists, the southern section is fixed by seawalls (100 m long) and the northern dune is protected by sand fences (Fig.1C). However, except in the very southern end of the beach, the effect of management strategies on the sediment budget can be considered as negligible (Biausque et al., 2017; Biausque et al., 2018, in press).

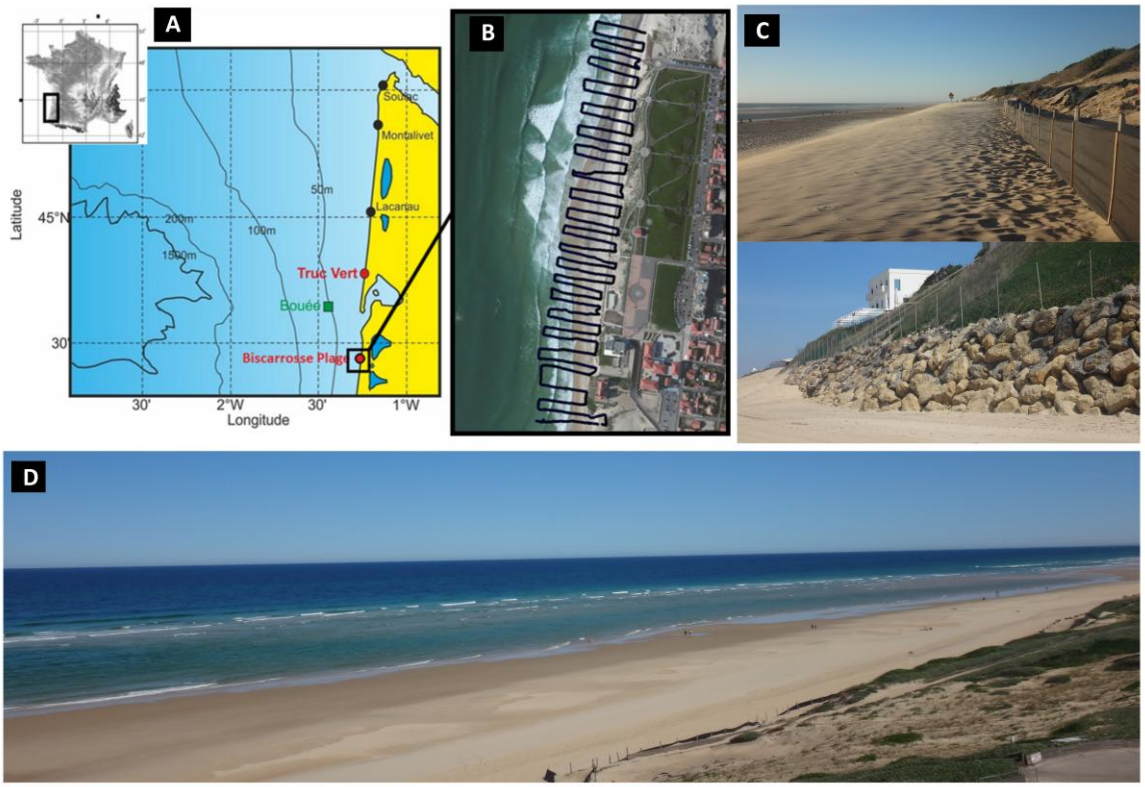

Figure 1: (A) Biscarrosse Beach location on the South-West French Atlantic coast. Offshore conditions were extracted at location 'Bouee' indicated with the green mark. (B) Example of current topographic survey undertaken at Biscarrosse Beach with the location of the cross-shore profiles. (C) Sand fences deployed in the northern part of the beach (up) and seawall deployed in the very southern part (down). (D) Overview of the northern end of the dune, the beach and the inner sandbar.

2. Topographic Surveys

From November 2015 to October 2017, more than 130 DGPS walked surveys were recorded. Here we will focus only on the two winter periods (2015/2016 and 2016/2017) and the summer period in between the two. Covering an alongshore distance of 700 m and extending from the dune to the low tide limit, 30 transects with alongshore spacing of 20 m and cross-shore spacing less than 1 m (one point saved per second) were collected at low tide using a Trimble® R6 DGPS system with an accuracy of 0.010 m (± 0.002 m) horizontally and 0.020 m (± 0.002 m) vertically (Fig. 1B). During summers and due to the presence of specific beach structures, such as cusps, the number of

transects could increase up to 50. To obtain the topographic maps, an interpolation is done following the method previously used on the Truc Vert beach (40 km north from Biscarrosse, Castelle et al., 2007), on a grid of 0.5 m by 0.5 m. This methodology provides data on beach morphology and dune evolution at short timescale, in particular before, during, after and in-between energetic events. A number of representative isocontours can then be extracted from interpolated topographic data, in particular the ones corresponding to the dune foot (Z=4.5 m), the supratidal (Z=2 m) and upper intertidal beach limits (Z=0.45 m), but also other proxies used to characterize the shoreline variations found in the literature for this area (Castelle et al., 2014 ; Senechal et al. 2015). The dune foot's isocontour is detected as the slope rupture between the dune and the beach; the supratidal beach is identified by the berm's limits and the inner bar by the MSL (Fig.2). Following the methodology proposed by Angnuureng et al. (2017) the shoreline is approximated by the elevation equals to +0.45m above the MSL, which correspond in our case to Z=0.85 m (Fig.2).

Volumes are also calculated for different sections of the beach (e.g. dune, supratidal and intertidal beach) with the purpose of tracking the evolution of each section and cross-shore volume fluxes. Moreover, the alongshore dimension is also characterized with the integration of an indicator developed by Burvingt et al. (2017) to estimate the longshore variation in the morphological response of the beach, the LVI. This parameter also indicates if there is a dominance, cross-shore or longshore, in the sediment transport direction: LVI=1 and respectively, if LVI=0, the transport is dominated by an alongshore (respectively a cross-shore) sediment transport.

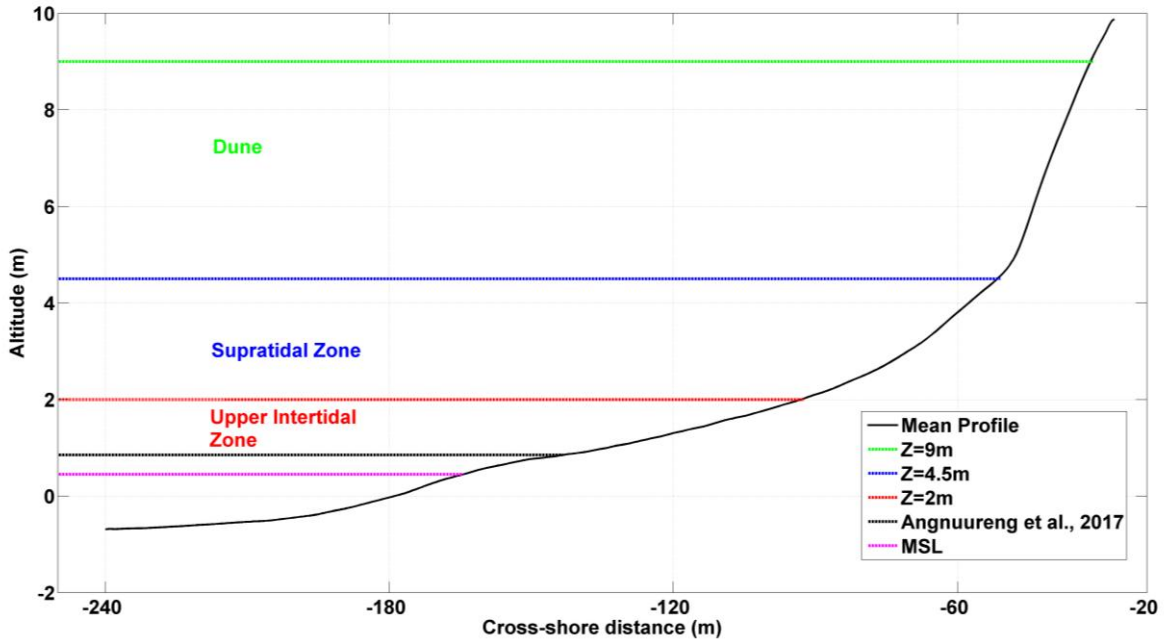

Figure 2: Mean beach profile (the 11th of March 2016 is taken as an example) and isocontours used as proxies and to determine the different beach sections limits.

3. Hydrodynamic data

Hydrodynamic datasets are extracted from two models. The tide is provided by the model developed by the SHOM Institute which lays out a node at Biscarrosse, and offshore waves extracted from the Marc model based on WaveWatch3. The modelled wave node is 50 m deep, offshore of the Cap Ferret sand spit (Fig.1, green square). Following the approach proposed by Dolan & Davis (1994) and previous definition for this area (Senechal et al., 2015; Angnuureng et al., 2017), a storm event is defined when H_s exceeds 4 m ($H_{95\%}$) during a complete tidal cycle, meaning 12 hrs. A succession of two or more storms, where the 'calm' period between events is less than 5 days, is then considered as a cluster of storms.

Following the linear approach, wave energy flux (P_{tot}) has been estimated in 50 m water depth as:

$$P_{tot} = \frac{1}{8}\rho g H_s^2 C_g \qquad \text{Equation 1}$$

where C_g is the wave group velocity (Eq.2), H_s the significant wave height, ρ the density of the ocean's water (1025 kg/m^3) and g the gravitational acceleration (9.81 m/s²).

$$C_g = \frac{1}{2}\, c\left(1 + \frac{2kd}{\sinh 2kd}\right) \qquad \text{Equation 2}$$

where c is the phase velocity (Eq.3),

$$c = \sqrt{\frac{g}{k}\tanh kd} \qquad \text{Equation 3}$$

and k the wavenumber and d the depth. The wavenumber k has been calculated by resolving the linear dispersion relation, using a Newton iterative method.

The longshore component of the energy flux has then been calculated as:

$$P_y = P_{tot}\cos\theta \sin\theta \qquad \text{Equation 4}$$

where θ is the incidence angle of the wave.

In order to better assess the chronology of the different energetic events, the wave energy flux has then been normalized by the total wave energy flux for each winter season. Then the cumulative normalized wave energy flux P has been calculated.

Finally, the normalized wave power (P_n) is calculated following the equation proposed by Morris et al. (2001):

$$P_n = P\frac{\eta_{dtr}}{\eta^*_{dtr}} \qquad \text{Equation 5}$$

were P is the wave energy flux (or wave power) and η_{dtr} the daily tidal range in relation to the maximum spring tidal range η^*_{dtr} .

Results

1. Winter Conditions

1.1 General overview

Fig. 3 represents the wave conditions over the complete study period from November 2015 to May 2017. We clearly observe a strong seasonality in the wave conditions with energetic waves (generally H_s > 2 m) associated with longer periods (Tp ~ 12 s) occurring during the winter periods, typically from November to April, and much weaker conditions (generally H_s < 2 m) associated with shorter periods (Tp ~ 9 s) during the summer period, from May to October. Data show that both studied winter periods started at the beginning of November, with the first winter storm conditions associated with H_s exceeding 4 m, and finished in the middle of April.

However, looking further in detail, data indicate that wave conditions were quite different between the two winters. Table 1 provides an overview of the characteristics of these two winters. Data indicate that the median ($H_{50\%}$) and mean significant wave heights are higher during the first winter (2015/2016) of the studied period by a factor of nearly 1.4, while the maximum experienced H_s is similar for the two periods (variation by less of 3% between the two winters). In terms of energy, both the mean and cumulative wave energy are also greater in 2015/2016 by a factor of nearly 1.7. However, the maximum observed energy flux was observed during the second winter period.

The ratio P_y by P_{tot} reflects the longshore energy flux compared to the total energy flux. During the two winters, this ratio never exceeded 50% but the number of peaks surpassing 20% is multiplied by 3 during the second winter season in 2016/2017, and concentrated during the less energetic periods.

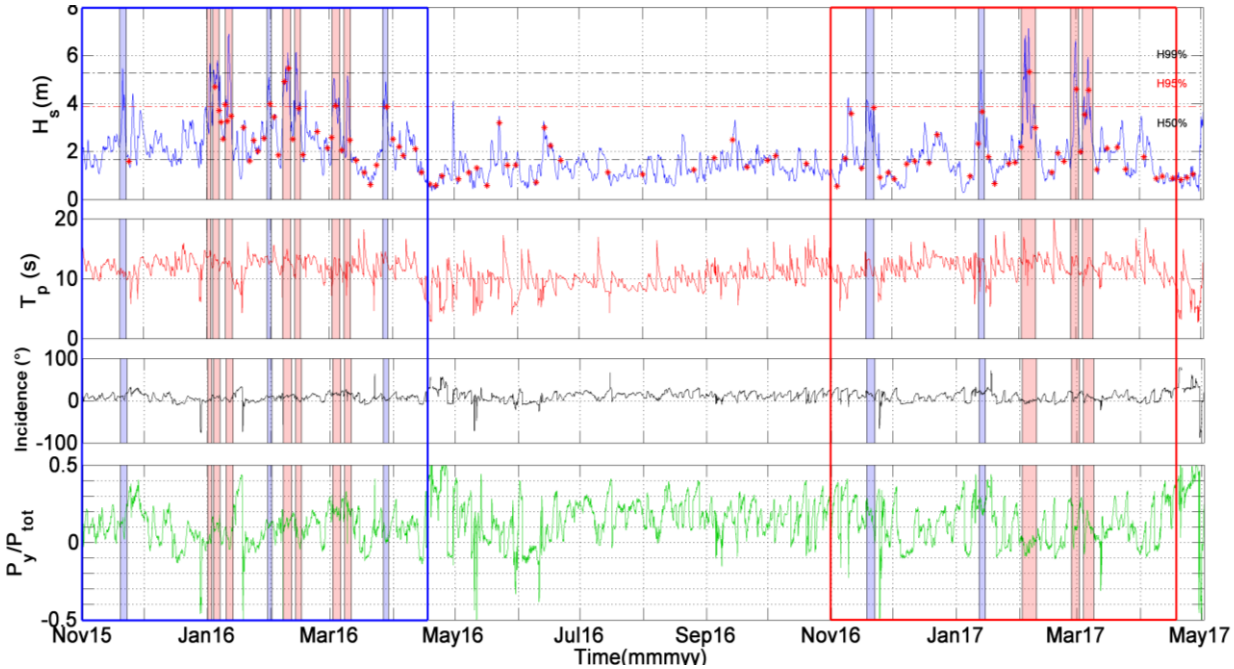

Figure 3: Hydrodynamic conditions: significant wave height (H_s), Peak period (T_p), Wave incidence relative to the beach orientation and Ratio of the alongshore wave energy flux (P_y) on the total wave energy flux (P_{tot}). $H_{99\%}$, $H_{95\%}$ and $H_{50\%}$ are calculated over the total period. Red crosses represent the surveys.

	Winter 2015/2016	**Summer 2016**	**Winter 2016/2017**
H_s maximum (m)	6,89	4.1	**7,13**
H_s mean (m)	**2,49**	1.34	1,89
$H_{50\%}$ of H_s(m)	**2,27**	1.28	1,68
T_p max (s)	18,2	**17,2**	**20,0**
T_p mean (s)	11,9	10,0	11,8
T_p median (s)	12,2	10.1	12,2
C_g maximum (m/s)	18,7	18.07	**19,7**
Mean Energy (J)	**9346**	2588	5995
Cumulative Energy (J)	**$3,84.10^7$**	$1,21.10^7$	$2,44.10^7$

Mean Energy Flux (W/m)	**$1{,}17.10^5$**	$2{,}43.10^4$	$0{,}74.10^5$
Maximum Energy Flux (W/m)	$7{,}97.10^5$	$1{,}56.10^5$	**$9{,}70.10^5$**
Total Energy Flux (W/m)	**$4{,}80.10^8$**	$1{,}14.10^8$	$3.02.10^8$
Mean Wave Steepness	**0,012**	0.0095	0,009

Table 1: Winters general characteristics: significant wave heights (H_s), peak periods (T_p), wave group velocity (C_g), wave energy and wave energy fluxes and the wave steepness.

1.2 Storm activity

Table 2 provides an overview of the storm activity during the two winters. The number of storms observed during the first winter in 2015/2016 (10) is twice the number of storms observed during the second winter in 2016/2017 (5). Furthermore, storm intensity in terms of significant wave height and storm duration was also greater during the first winter. Thus, the $H_{95\%}$ was 4.91 m for the 2015/2016 period, which is 0.91 m above the generalized $H_{95\%}$ calculated in previous studies (e.g. Senechal et al., 2015), while in 2016/2017 it was 0.10 m below. Furthermore, the maximum storm duration observed during the first winter was 81 hrs and only 44 hrs during the second winter. Data also indicate that three clusters were observed in the first winter: two of them included 2 storms and one 3 storms, while during the second winter period, only two 2-storms clusters were observed.

	Winter 2015/ 2016	**Winter 2016/2017**
Number of storms	10	6
Number of clusters	3	2
Number of 3-storms cluster	1	0

Maximum storm duration (hrs)	81	44
Mean storm duration (hrs)	36	28
Total Storm duration (hrs)	359	167
$H_{95\%}$ of H_s (m)	4,91	3,87

Table 2: Winter storm characteristics: number of storms, storm durations and $H_{95\%}$

2. Morphological evolution

2.1 General overview

Fig. 4 compares the beach morphology between the two years, before (A) and after each winter season (B). Panels A and B are structured following the same schema: the top panel is the morphology prior to the beginning of the first winter period, namely 2015/2016 (respectively after the first winter period, panel B), the middle panel is the morphology prior of the beginning of the second winter period, namely 2016/2017 (respectively after the second winter period, panel B), and the lower panel is the difference between the two previous panels. Thus, the lower panel represents the difference in morphology between the two years prior to the winter season (A) and after the winter season (B). Finally, the bottom panel represents the alongshore averaged mean profiles for each topography previously described. According to the Fig. 4A, the beach morphologies can be considered similar before the two winter periods: in the two cases, the morphology was uniform alongshore and the differences in elevation between the two years $|\Delta z|$ are lower than 0.2 m for the entire study zone. This is further highlighted with the alongshore average profiles that show similar shape and elevation between the two years. In contrast, the post-winter profiles (panel B) are quite different, essentially for the lower part of the beach. According to the morphological evolution, differences are observed both in the alongshore and cross-shore distances. In particular, the lower intertidal zone at the end of the second winter is lowered compared to the one at the end of the first winter (nearly 0.5 m on average), highlighted by the comparisons between the two alongshore averaged profiles. The upper part of the intertidal beach exhibits a strong alongshore variability

between the two years: after the second winter the northern end of the upper intertidal beach is lower (by nearly 1 m) while the southern end is much higher (by nearly 1 m). These alongshore uniformity is being smoothed in the alongshore averaged profiles.

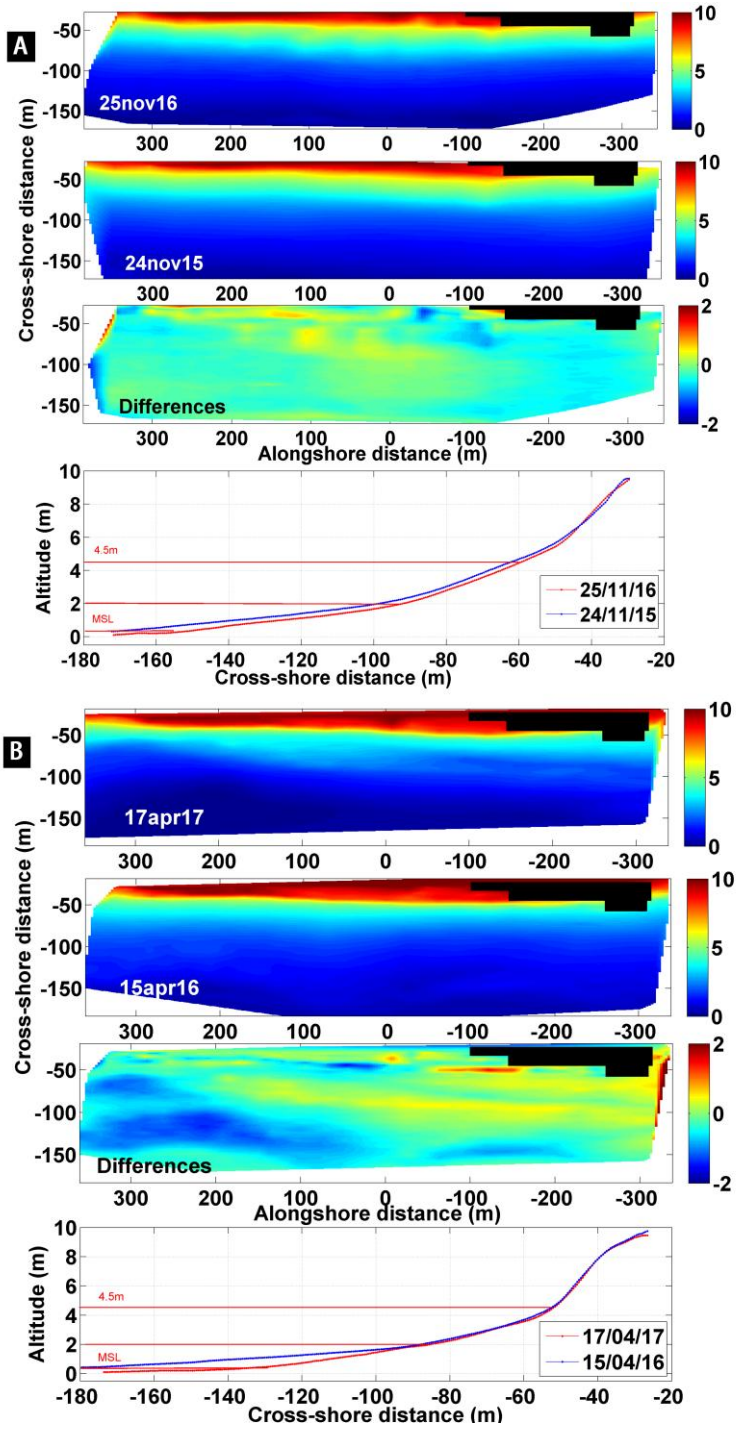

Figure 4: Comparison between 2015/2016 and 2016/2017 pre-winter (top) and post-winter (bottom) beach morphologies and mean profiles

In Fig. 5 we focus on the seasonal response of the beach for each winter season. Here the figure represents (left) the observations for the first winter season (2015/2016) with, respectively, from top to bottom: the topography prior to and after the winter season, the difference between the two surveys and the alongshore averaged profiles corresponding to the two topographic surveys displayed above, and (right) the same figures but corresponding to the second winter period (2016/2017). After the winter 2015/2016 the alongshore averaged profile highlights a lowering of 1.5 m of the upper part of beach (between isocontours Z=2 and 4.5 m), however 3D morphologies indicate that it results from significant non-uniform patterns: the southern section is two times more eroded than the northern end section. In contrast the lower beach is relatively stable, even accreted, and is alongshore uniform. The mean profiles (Fig.5; left bottom panel) illustrate a dune foot retreat (isocontours 4.5 m) of about 15 m associated with beach erosion. After the winter 2016/2017 we also observe an overall lowering of the upper part of the beach (1.0 m) but to a lesser extent than the previous winter (30% less). In contrast to the winter 2015/2016, alongshore averaged profiles indicate an overall lowering of the intertidal zone. 3D morphologies however highlight that it results from significant alongshore variability: in the central part of the beach the erosion is less than 1 m while it reaches 1 m (and more) in the northern end of Biscarrosse beach. In the southern end however the lower beach and the upper intertidal part are accreted.

The volume variations calculated between the first and the last days of the winter, for the entire beach (0.85 - 9 m), are not significantly different for the two winter seasons: -26.7 m^3/m for the first winter *vs.* -26.3 m^3/m for the second winter.

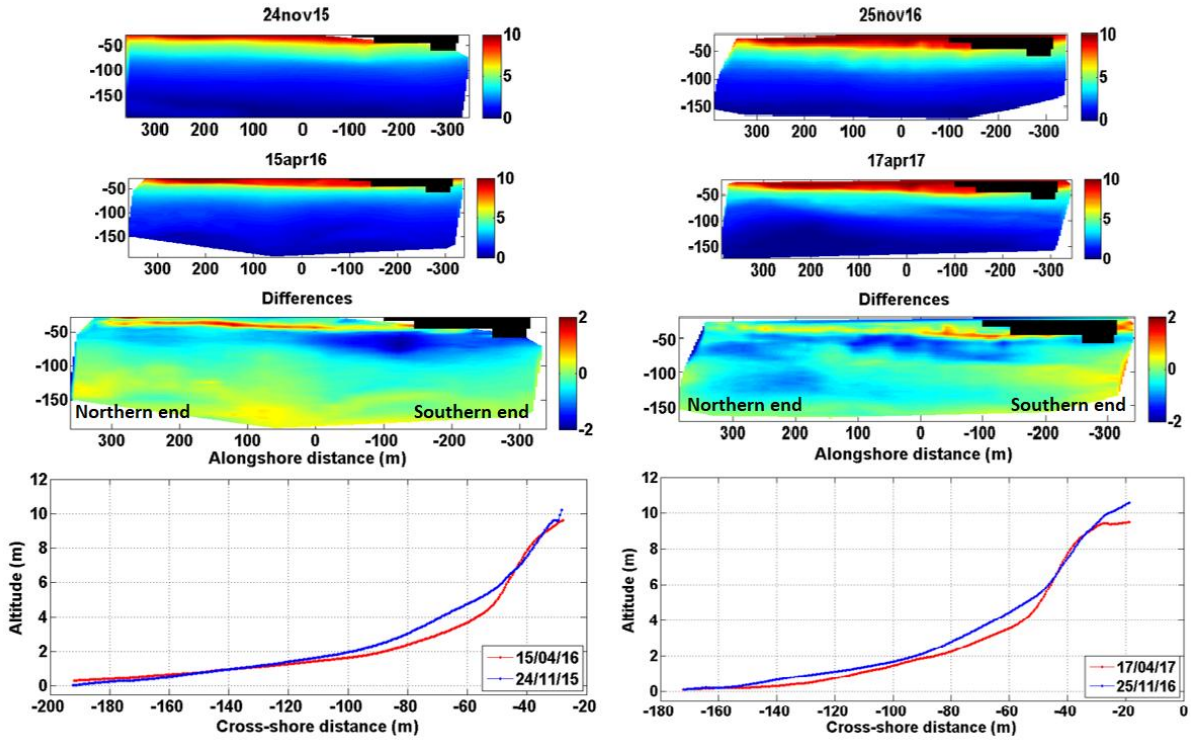

Figure 5: Morphological evolution and mean beach profiles between and after the winters 2015/2016 (left) and 2016/2017 (right).

3. Multi-proxies beach response

3.1 Isocontour dynamics

Here the focus is to provide further insight in the response of the beach system by analysing the dynamics of different beach sections: dune, supratidal and intertidal beach. Fig. 6 illustrates the time-evolution of the alongshore averaged positions of different proxies described previously. Data clearly show the seasonal pattern in the dynamic of the dune foot and the berm: an overall erosion (onshore retreat) is observed during the winter period (typically Nov-March) at the end of which, the berm reaches the cross-shore position -80 m (zero being landward) and the dune foot the position -50 m while during the summer period, they both progradate to the cross-shore positions -105 m and -70 m

respectively. The range of variation for these two proxies is of the same order for the two winter periods considered in this study: 15-20 m for the dune foot and 20-25 m for the berm. A time-lag between the supratidal beach/berm recovery and the dune foot recovery is also observable: the supratidal beach/berm reaches its pre-winter position in the middle of the summer (July) while the dune foot recovery is delayed by nearly 2 months. The inner bar dynamics also show a strong seasonal pattern characterized by an overall offshore migration during the winter period probably associated with an up-state transition and an overall onshore migration during the summer period probably associated with a down-state transition. Besides, data do not reveal any significant difference here between the two winters: the overall winter seasonal cross-migration of the inner bar is about 40 m and the proxies reach the same seasonal limits.

However, data also illustrate that the event timescale is highly significant, the short-term evolution (a few days) can be of the same order in magnitude as the seasonal evolution (15-20 m). Pink and blue patches on Fig. 6 highlight storm clusters and isolated storms, respectively, coded from E1 to E9. For example, during the event E3, both the dune foot and the supratidal beach (4.5 and 2 m) experience onshore retreat by an order of 15 m.

Data also indicate that the upper part of the beach (dune foot/supratidal beach) and the lower part of the beach can evolve in an opposite way to a same event. For example, during the first event (E1, Fig. 7) isocontours Z=2 and 4.5 m moved landward (erosion) while Z=1 and 0.85 m moved seaward (accretion or up-state transition of the bar) suggesting cross-shore sediment transfers. The example of event 3 (E3) implies the same tendency, nevertheless the intertidal beach experiences both accretion then erosion for the same event, whereas the supratidal zone is only eroded, and the dune foot retreated. Interestingly, focusing on the berm proxy (2 m) the short-term dynamics are very different between the two winter periods. Thus, during the first period we observe a clear storm/post-storm signal: the berm is generally eroded during the cluster and recovers between clusters. This pattern is not clear during the second winter period.

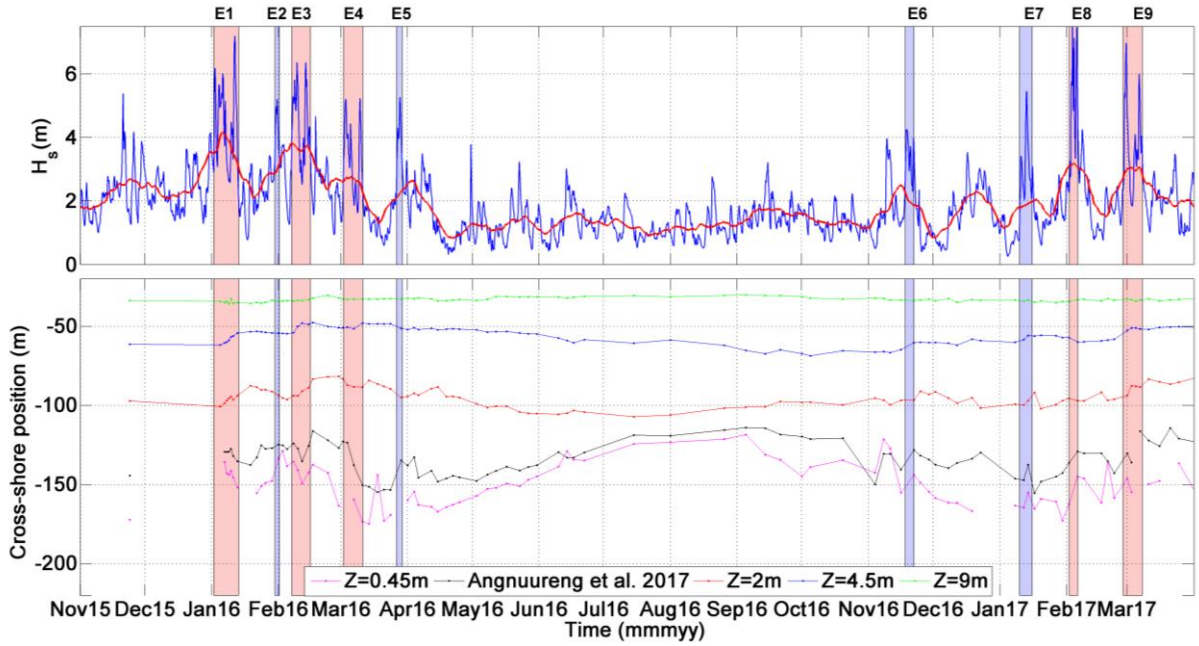

Figure 6: Significant wave height (top) and cross-shore dynamics of selected isocontours (bottom) representative of different sections of the beach: pink (dune), green (dune foot), blue (berm), black and red (lower intertidal beach)

3.2 Volume variations

In many previous studies that address storm beach evolution, the sediment volume is calculated for the entire beach profile, mainly above MSL (e.g. Vousdoukas et al., 2011), not allowing for the investigation of cross-shore exchanges within the dune/beach system itself. In Fig. 7, a multiproxy approach is proposed here with a study of the dune, supra- and intertidal beach separately. At the end of the first winter season (blue square, Fig.7), the dune volume (in green, Fig. 7) is lower than before the winter (-6 m^3/m), while the supra- and intertidal beach post-winter volume equal the initial pre-winter one (in blue and red respectively, Fig.7). Besides, the dune sediment volumes are only poorly correlated (with a correlation coefficient of 0.14, significant at the 98% confidence level) with the supratidal beach variations. However, the supra- and intertidal zone are negatively

correlated (-0.54), suggesting sediment exchanges. Thus, even if fluctuations occurred during the winter 2015/2016 the total sediment balance seems stable for the beach (blue arrow). The winter season is followed by a seasonal recovery period extending from May to August 2016 associated with an increase of the supratidal beach volume and a decrease of the intertidal beach volume. During the second winter (red square, Fig. 7) the dune has lost sediment more progressively, throughout the season. As in 2016, sand volume variations are visible for the beach (supra- and intertidal) but, in this case, the final volume is inferior to the initial one (-2 m^3/m compared to the initial position). A general erosional tendency for the three different cells is highlighted by the red arrow in Fig. 7.

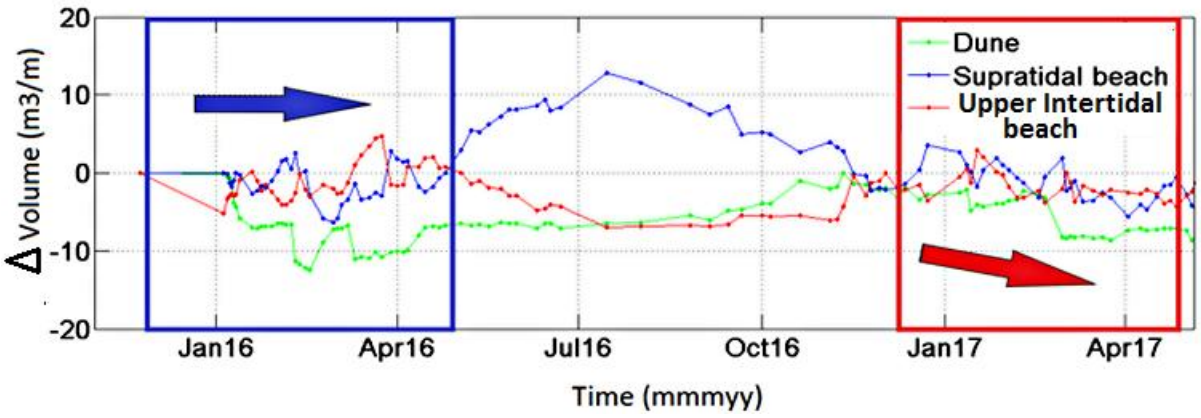

Figure 7: Beach volume changes compared to the 24th of November 2015

3.3 Volume variations versus isocontours positions

Fig. 8 compares the potential correlations between the variations in volumes and different cross-shore positions: the volume evolution of the upper intertidal beach and its corresponding isocontour, Z=MSL (A), the volume evolution of the supratidal beach and its corresponding isocontour, Z=2 m (B), the volume evolution of the upper intertidal beach and its upper isocontour limit, Z=2 m (C), the volume evolution of the supratidal beach and its upper isocontour limit, Z=4.5 m (D) and the volume evolution of the entire beach and the isocontour Z=MSL (E). The panel F represents, with mean profiles, the evolution of the beach over one year, from January 2016 to December 2016.

According to the panels A and B, volumes of the beach zones and their corresponding isocontours are correlated, with a correlation coefficient of, respectively -0.71 for the MSL/upper intertidal beach and -0.72 for the Z=2 m/supratidal beach. Those correlations indicate that an onshore retreat of the isocontours is related to a decrease in volumes. Moreover, the volume evolution of the upper intertidal beach is also correlated to the position of the isocontour Z= 2 m with a coefficient of 0.63 (C), revealing that the volume of the upper intertidal beach is also linked to the position of its upper isocontour. This suggests that when the volume of the upper intertidal beach increases, its upper limit (2 m) is moving onshore while its lower limit (the MSL) is moving offshore: the width of the upper intertidal beach is increasing. In contrast, the isocontour of the MSL and the volume of the entire beach (E) are not correlated at all, asking the question of the representativity of those two proxies currently used in the literature.

Nevertheless, in contrast, the supratidal beach volume evolution is not significantly correlated (-0.23) to the position of the isocontour Z=4.5 m (D). As highlighted in panel (Fig. 8F), this observation seems to be due to the berm reconstruction during the summer. Indeed, the isocontour 4.5 m is barely moving offshore, but the volume increases considerably. Thus, the upper intertidal beach volume increase is directly linked to a width increase of the zone, while an increase of the supratidal beach volume could be linked to an elevation of the altitude of the profile.

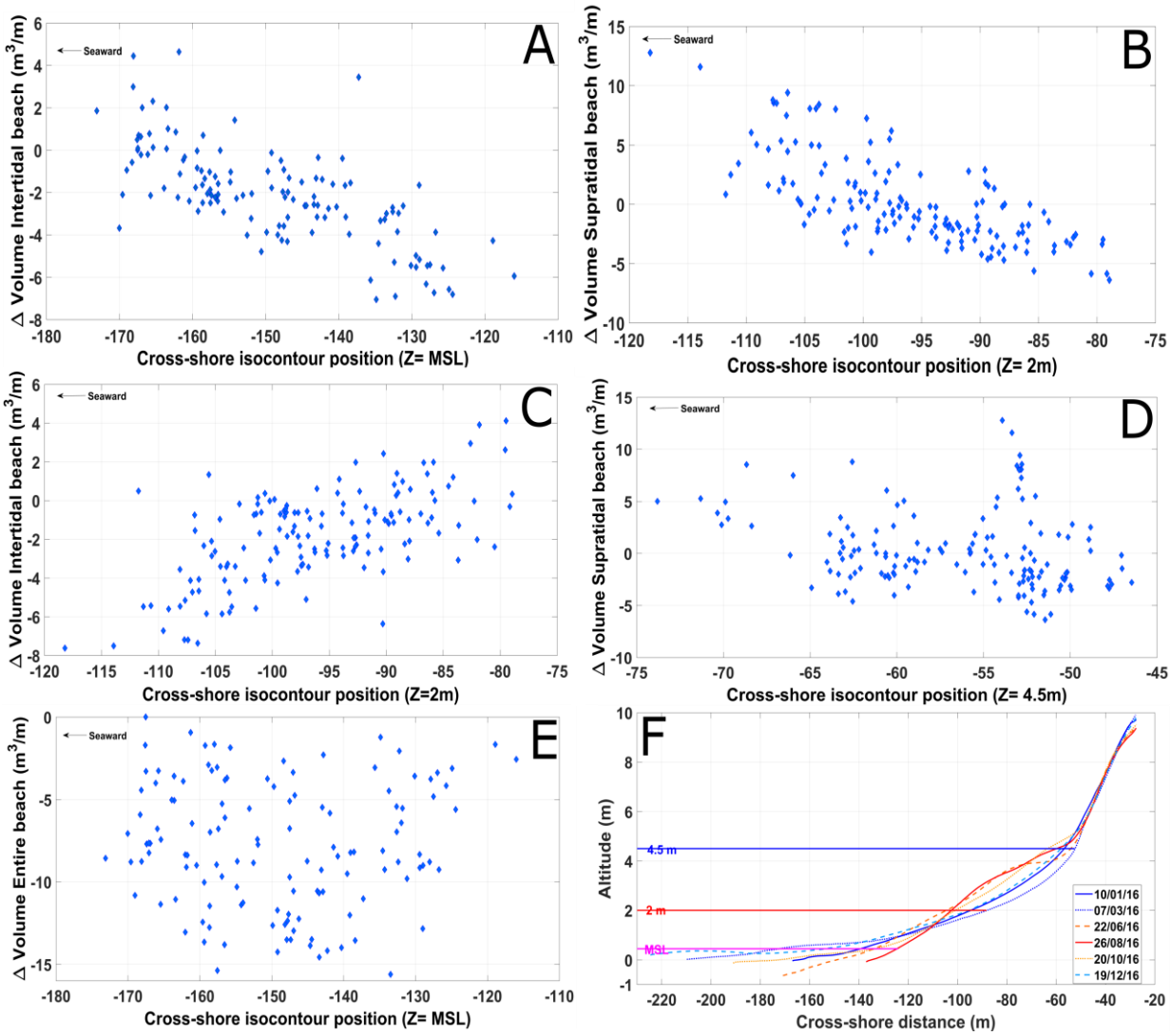

Figure 8: Comparisons between isocontours and volumes (A: Upper intertidal beach volume vs. MSL position; B: Supratidal beach volume vs. z=2 m position; C: Upper intertidal beach volume vs. z=2 m position ; D: Supratidal beach volume vs. z=4.5 m position ; E: Entire beach volume vs. MSL position); alongshore averaged profiles of the beach covering one year (F).

Discussion

Here we present an original data set of high-frequency topographic surveys (at least 2/week) over an 18-month period spanning two winter seasons. Table 3 summarizes some of the key values presented in the results section. One of the key results is that despite similar pre-winter beach morphologies (Fig. 4) but contrasting hydrodynamic conditions (Table 1, 3), the cumulative wave energy flux was 1.7 times higher during the first winter season), the sediment budget of the

dune/beach system is nearly the same after the two winter periods. Data also indicate that the cross-shore displacements of the different proxies: dune, berm and bar are of the same order for the two winter seasons and consistent with previous works on the area (e.g. Senechal et al., 2015; Angnuureng et al., 2017) and that they reach the same cross-shore limits during the two winter seasons. This, of course, raises intriguing questions as, from a management point of view, the beach morphology before the winter period and the cumulative hydrodynamic conditions during the winter period are supposed to provide useful inputs to forecast the post-winter beach morphology (e.g. Baart et al., 2015; Reeve et al., 2016).

	Winter 2015/2016	**Winter 2016/2017**	**Differences between the two years (%)**
ΔVolume	-26,7m^3/m	-26,3m^3/m	1.5%
Energy	3,84.10^7J	2,44.10^7J	37%
Proxies displacements	15-20m	15-20m	0%

Table 3: Differences in sediment budget over the winter period, cumulative energy for each winter period and maximum proxies cross-shore displacements for each winter. The difference between the two years are provide in percent.

1. Energy sequence

The Fig. 9 evidences the cumulative absolute values of the wave energy flux for winter 2015/2016 (in red) and winter 2016/2017(in blue). According to the Fig. 9, the winter 2016/2017 began early in the season compared to the previous winter. Indeed, the wave energy flux of the winter 2015/2016 starts to increase in the middle of November while that of the winter 2016/2017 had already reach 16% of its total for the same period. This suggests that even if the total energy experienced during the first winter (2015/2016) is higher than that experienced during the second winter (2016/2017), it results from an overall increase in wave conditions, even during weaker conditions compared to

storm conditions. In contrast, during the second winter we observe a succession of energetic events with very calm conditions in between. So, during the first winter, the cumulative flux increases progressively until January and the most energetic event during the period, accounting for 20% of the total energy flux (first red arrow), occurs relatively early in the winter season (beginning of January) followed one month later by the second most energetic event, accounting for slightly less than 20% of the total energy flux. Further, between these energetic events the energy fluxes gradually increase. During the second winter, the evolution is significantly different. The most energetic event accounting for 20% of the total flux occurs at the beginning of February, followed one month later by two energetic events whose intensities, taken separately, are however two times smaller than the most energetic ones. Data also indicate that between these periods, the wave conditions are extremely weak.

This difference in wave energy chronology within the season raises the question of wherever or not it could have a significant impact on the beach response as previously suggested (e.g. Dissanayake et al., 2015; Senechal et al., 2017; Brooks et al., 2017), in particular on the initiating of the recovery periods. Indeed Philipps et al. (2017) showed that the recovery process is generally a gradual process that requires sufficient energy levels to be initiated: sediment migrating back to the beach, onshore bar migration, onshore bar welding and then finally sediment supply to the upper beach.

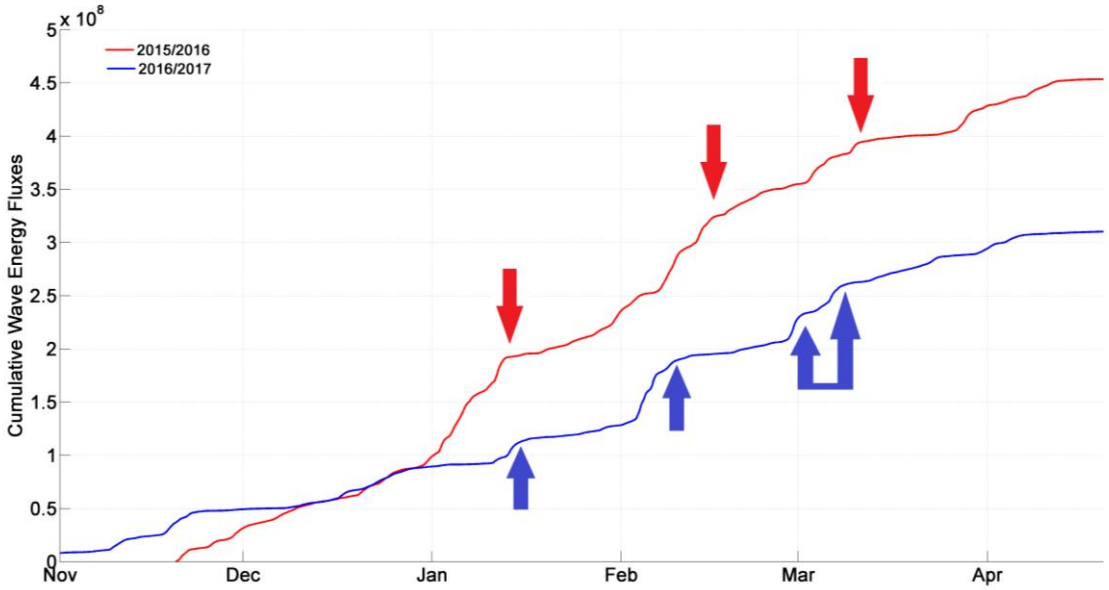

Figure 9: Cumulative wave energy flux for the winters 2015/2016 (red) and 2016/2017 (blue). Arrows highlight energetic events.

Finally, the tide might have play a crucial role in the response of the beach (e.g. Almar et al., 2009; Vousdoukas et al., 2012; Masselink et al., 2014; Coco et al., 2014). Fig. 10, panel B, displays the normalized wave power (Pn) proposed by Morris et al. (2001) and used by Loureiro et al. (2012). This parameter is used to look at the enhanced erosion potential linked to spring tide periods compared to neap tides, without neglecting the possible erosion resulting from storm conditions under lower tidal ranges. For low values of normalized wave power (P_n<1.5 $Jm^{-1}s^{-1}$), mainly linked to a low water level (neap tide periods), storm waves do not seem efficient enough to erode the supratidal beach: the upper intertidal beach is lowered and the supratidal volume increases (E2, E5, E6 Fig.10). On the other hand, storms correlated to P_n higher than 2 $Jm^{-1}s^{-1}$ linked to high water level (due to spring tide periods and/or high energy fluxes), generate a visible erosion of the dune and the supratidal beach with a possible recovery of the upper intertidal beach (E1, E3, E7, E9, Fig.10). Thus, if the water level at spring tide is high, the erosion of the supratidal beach will be significant, but the offshore export of the sediment might be reduced as result of less effective undertow under higher water column.

Further, calm hydrodynamic conditions during high water level at spring tide might not induce recovery especially if associated with large wave incidence (e.g. Coco et al., 2014).

Nevertheless, the water level plays a key role based on thresholds that define the part of the beach that will be touch by an event: high P_n values (storm conditions and spring tide) are linked to an erosion of the upper part of the system with possible deposition in the lower part of the beach, medium P_n values (storm conditions or spring tides) seem necessary to initiate a sediment movement from the upper intertidal beach toward the supratidal beach. Moreover, the post-storm recovery is only possible for sufficient P_n values (around 1 $Jm^{-1}s^{-1}$): during the first winter, the post-storm recovery is efficient, but during the second winter P_n values are to low (conditions to calm) to generate an effective recovery.

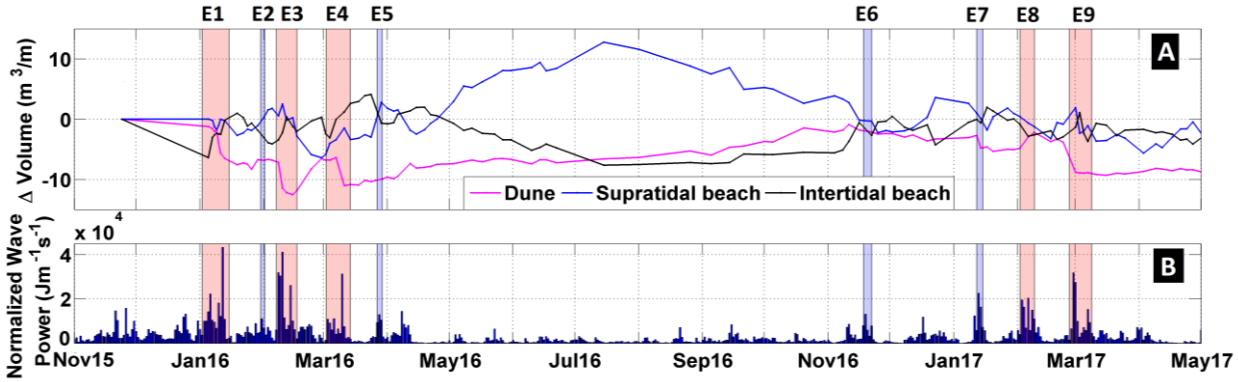

Figure 10: Volume evolution of the tree beach zones (A), Normalized wave power (B).

2. Short-term storm response

Looking at the event timescale (Fig.6), storms within a cluster mostly result in erosion. Fig. 11 provides detailed insight into the four main erosive events. After the first cluster 2016 (E1, Fig.11), a dune foot retreat associated with an erosion of the supratidal beach (above 1 m) is observable as well as for the intertidal beach (Fig.11; left top panel). The cluster of February 2016 (E3) also results in an overall erosion of the supratidal beach and the dune (-1.5 to 2 m). The last cluster of the season 2015/2016 (Fig.11; left bottom panel) erodes mainly the dune foot and the higher beach (< -1 m) but accretion in the lower and intertidal beach is also observed (< +1 m). During the winter 2016/2017,

only the last cluster E9 significantly erodes the dune/beach system. Erosion in these four cases is systematically centered on the upper beach while the lower beach can either erode or accrete depending on the event.

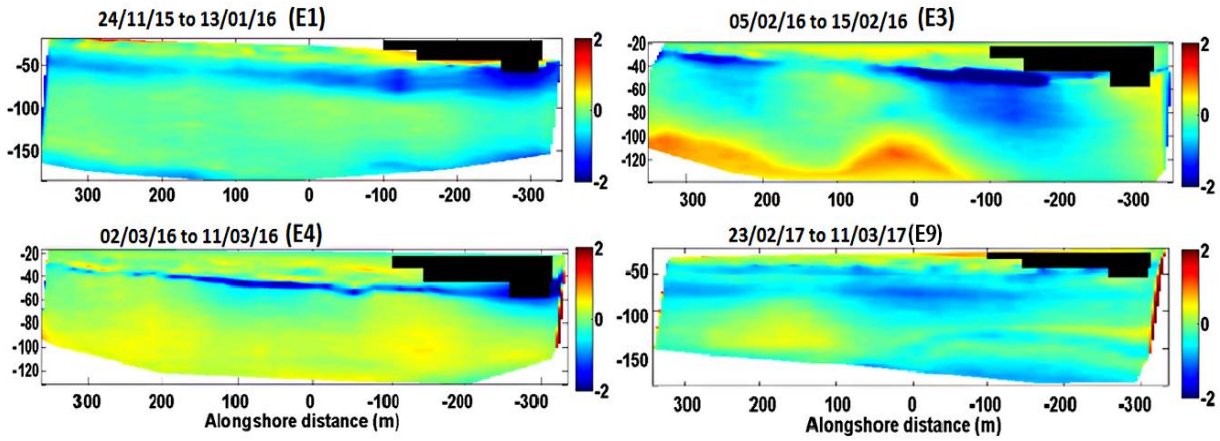

Figure 11: Morphological evolution (elevation difference in m) of the beach during erosive events

Interestingly, however, is that our data also indicate that recovery or limited erosion is also observed during energetic events classified as storm events, consistent with previous observations (e.g. Coco et al., 2014). This is, for example, the case for events E2, E5 during the first year: we observe that the recovery process initiated just at the end of the previous storm event is not interrupted during these two events (Fig. 6); similarly, during event E8, although being the most energetic of the second winter season, no erosion is observed. Fig. 12 provides further insight into the four storm events associated with no-erosion or recovery of the beach. In those four cases, the upper beach recovered while, similarly to the erosive cases, the lower intertidal beach displayed contrasting evolution (either erosive or accretive). Recovery of the lower beach plays a key role in the upper beach recovery (Senechal et al., 2009; Philipps et al., 2017; Brooks et al., 2017). Data indicate that it is highly variable but can be observed during energetic events.

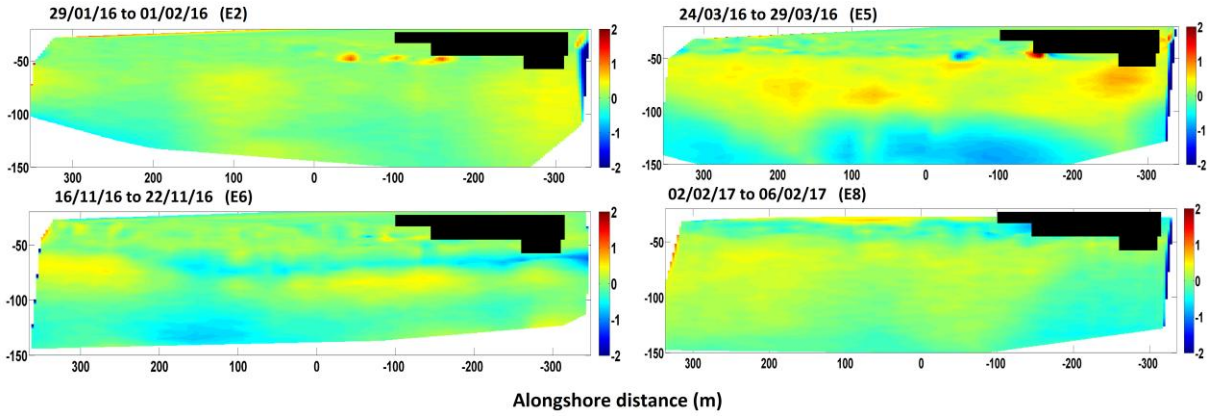

Figure 12: Morphological evolution in presence of storm conditions but associated with gain of sediment and characterized as recovery periods.

3. Recovery periods

Periods of recovery of the lower and upper beach seem here to play a crucial role in the dynamics of the beach at the seasonal timescale. In particular, their chronology during the winter season may explain why despite more energetic conditions during the first winter, similar sediment budget was observed with the second winter. As underlined previously, both winters experienced erosive and 'recovery' storm events (E2, E5, E6, E8). However, for the winter 2015/2016, the first recovery event (E2) was included between two massive erosive ones, while the second 'recovery storm' (E5) ended the winter season. In contrast, in 2016/2017, the first recovery event (E6, Fig.12) opened the winter season. Furthermore, the high frequency survey strategy adopted here allowed us not only to study each energetic event but also the evolution of the systems between events. Thus, our dataset also highlights the fact that the seasonal response of the beach depends on the periods between storms too, consistent with Brooks et al. (2017). However, here the typical timescale is within the winter period: in the case of the first winter, a post-storm recovery clearly takes place between each event, which is not visible for the second winter season (Fig.6). This supports the idea that the extremely calm hydrodynamic inter-storm conditions of the second winter season in 2016/2017 (Fig.9) were not sufficient to initiate the upper beach reconstruction (Scott et al., 2016; Philipps et al., 2017).

Indeed, during the winter 2015/2016 an overall seaward movement of the intertidal and supratidal beach is noticeable after each event (E1, E2, E3, E4, E5; Fig.6). In contrast, in winter 2016/2017, the erosion was extended between the events 7 and 8, and no recovery could take place. Thus, the first winter is characterized by a general erosive period from November to the middle of February, immediately followed by a recovery period that ended in the middle of July. In contrast, the winter 2016/2017 began with a short recovery time, followed, after January 2017, by a general erosion trend until April (Fig. 13). Consequently, the erosional volume rate resulting of the winters is the same, but it varies along the season: erosion partially compensated by a recovery period in the first case, whereas a progressive erosion period in the other one. One of the questions arising here is wherever the timing of winter is also important for the seasonal recovery: the early winter storms seems to allow for full recovery (winter 2015/2016 and summer 2016, Fig.13) while the seasonal recovery of the summer 2017 seems to be curtailed consequently to a delayedwinter season.

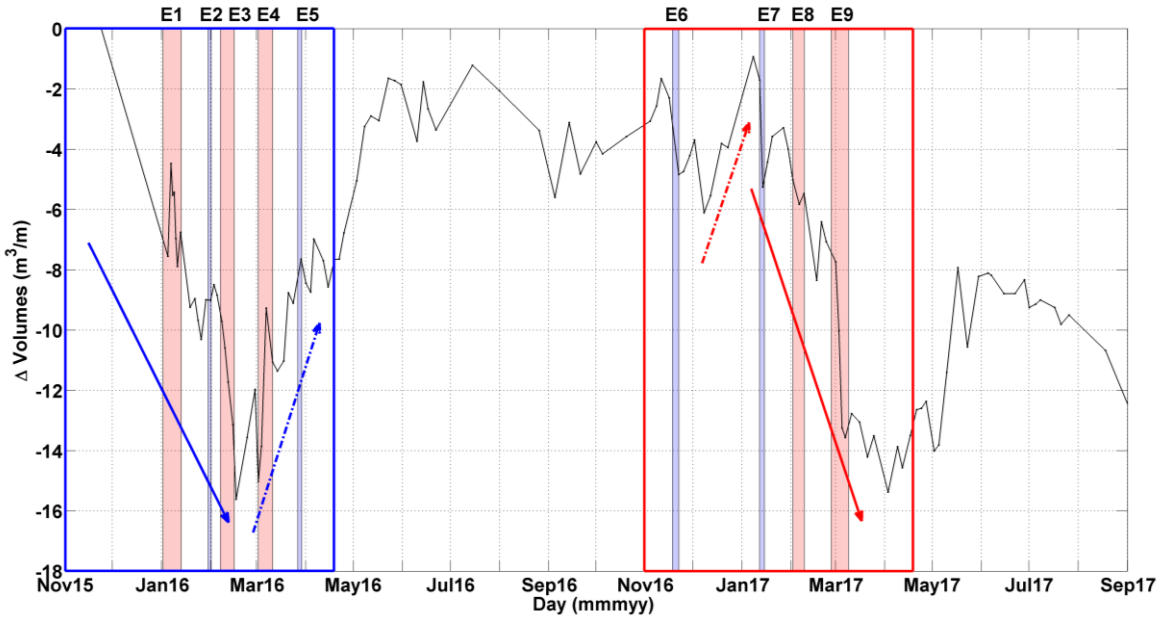

Figure 13: Beach sediment volume variations, calculated between the isocontours 0.45 m and 9 m, compared to the first survey (24th of November).

4. Sediment transfer processes

Data also suggest that the sediment transfers between the two winter seasons differ: during the first winter, the erosion of the supratidal beach is associated with an accretion of the intertidal beach, suggesting a sediment transport oriented mainly cross-shore from the dune to the sea (Fig. 5) while this is less evident during the second winter. The estimation of volumes of the separated zones of the beach (Fig.7) further supports the idea of a difference in the processes involved. Indeed, at the end of the first winter, the volumes of the intertidal and supratidal beach are back to their pre-winter positions assuming mainly cross-shore exchanges with limited sediments loss. For the winter 2016/2017, the final volumes of the two same beach cells is lower than before the season, implying a sediment loss from the system that could be linked to possible longshore sediment exchanges. Coco et al. (2014) reported that the largest measured erosive events in their data set were associated, amongst other factors, with strong longshore currents due to low energetic waves but with large wave incidence and spring tides.

Fig. 14 presents the volume evolution of the three zones of the system (A), and two parameters used to identify the alongshore component of the beach morphodynamics (C & D): the alongshore component of the wave energy flux (P_y) and the longshore variation in the beach response (LVI). P_y represents the alongshore wave energy flux and so the longshore sediment transport, via the alongshore current; high values of P_y reflect efficient alongshore currents that suggest an increase of the longshore sediment transport.

According to the Fig. 14, longshore wave energy fluxes are stronger during storm periods, but no significant difference could be detected between the two winters during the energetic periods. However, calmer periods of the first winter are characterized by higher values of P_y, compared to the second one. Biausque et al. (2018, accepted) showed that the recovery of the southern end of Biscarrosse beach is not only driven by cross-shore sediment exchanges, but also by longshore

transport. According to our observations, the post-storm recovery, mainly significant during the first winter, seems to be due to sufficient energetic conditions and significant alongshore currents.

Values of LVI over 0.8 (on average) highlight events that induced a longshore variability in the beach response morphology (e.g. E1, E5 or E9, Figs. 10, 11 & 13). But this indicator seems to be biased by the complexity of the study site (bars and rip currents, seawalls). Thus, some post-event morphologies of the beach exhibit high longshore variability despite moderate LVI values (e.g. E3, E4, Figs. 10 & 13). Moreover, a non-zero value of LVI can also be linked to an along-coast variation in cross-shore sediment transport (Burvingt et al., 2017). This phenomenon is currently observed on the Aquitanian coast because of the complex 3D morphology characterized by a crescentic offshore sandy bar and the presence of rip currents. For example, Castelle et al. (2015) report local dune erosion cause by cross-shore sediment exchanges that induced a strong alongshore variability in the response of the system to the winter 2013/2014. Thus, the LVI is not correlated to the P_y.

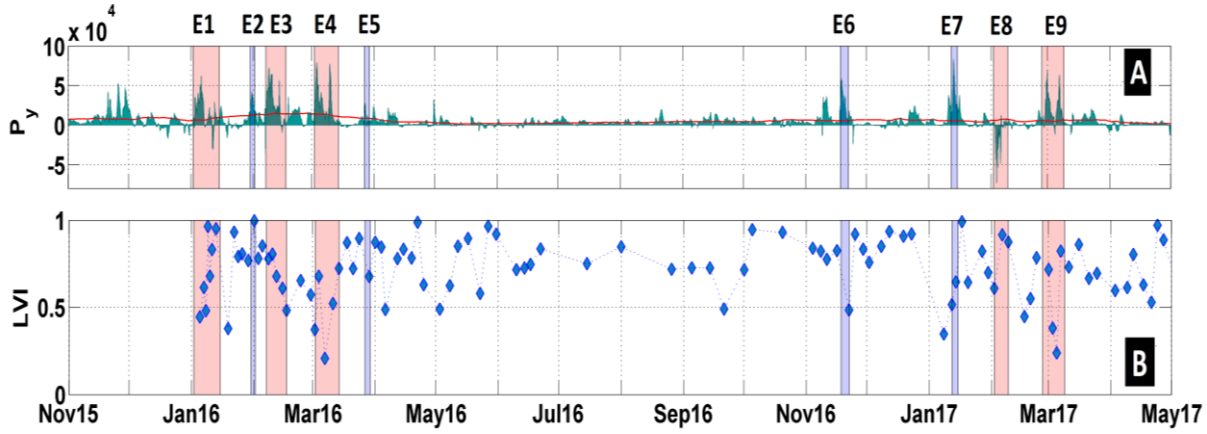

Figure 14: Alongshore wave energy flux P_y(A) and the longshore variation of the morphological response or LVI (B).

Although topographic surveys are limited to the intertidal and supratidal domains, reliable quantitative measures of the subtidal domain are necessary to allow for a reliable assessment of sediment budget (e.g. Philipps et al., 2017) or to evaluate wherever cross-shore or alongshore processes are dominant.

Moreover, Almar et al. (2009) showed that the inner bar dynamics were more sensitive to the tide than to the offshore wave conditions, especially because of the presence of the outer bar and the depth limited wave height in the intertidal area.

Conclusion

This study was conducted with the purpose of analysing the impact of short-term events on the seasonal response of an open sandy beach. High frequency DGPS surveys realized at Biscarrosse beach (SW France) allow the monitoring of the two consecutive winter seasons, respectively 2015/2016 and 2016/2017. Despite significant contrasting hydrodynamic condition levels but similar pre-winter morphology, the seasonal sediment budget between the two seasons was similar. The results suggest that the seasonal hydrodynamic conditions, characterized as wave height or wave cumulative energy, are not the only parameters driving the beach and dune morphological changes, and that the energy sequence is also a key driver. This is exacerbated by the short-term dynamics which impact seasonal trends. Indeed, energetic events (storms) are not always synonymus with erosional events and recovery can also be observed during these energetic events. Therefore, the sequencing of storms, meaning the succession of the events during the season, also plays a role in the impact of the winter period on the system and on the seasonal volume rate. Additionally, the use of multiple proxies to describe the shoreline evolution, such as the dune foot and representative isocontours above MSL, allowed better representation of the real morphological changes. Thus, the multiproxy method coupled to the high frequency methodology allow us to identify the possible post-storm recovery periods (between events) of the beach and the dune, which also play a key role in the response of the system to the next event. Post-storm recovery at Biscarrosse seems to be related to hydrodynamic conditions (as in the tide and the waves), but also to cross-shore and longshore sediment transport. Further analysis is requested to evaluate the impact on seasonal recovery and wherever or not the energy sequence is important during the summer period, in terms of morphological change.

Acknowledgements

Melanie Biausque is financially support by the Region Nouvelle Aquitaine. Data were collected thanks to financial support provided by the OASU (Observatoire Aquitain des Sciences de l'Univers), the SNO Dynalit (CNRS-INSU) and the OCA (Observatoire de la Côte Aquitaine). We would like to thank Tim Scott from Plymouth University who provided helpful feedback on the manuscript as well as Serge Suanez and Bruno Castelle for the stimulating discussions around the data set. We also would like to thank Carlos Loureiro and an anonymous reviewer, who provided many useful and valuable comments which significantly improved the manuscript.

References

Aarninkhof, S. G., Turner, I. L., Dronkers, T. D., Caljouw, M., & Nipius, L., 2003. A video-based technique for mapping intertidal beach bathymetry. Coastal Engineering, 49(4), 275-289.

Abadie, S., Butel, R., Mauriet, S., Morichon, D., Dupuis, H., 2006. Wave climate and longshore drift on the South Aquitaine Coast. Continental Shelf Research, 26(16):1924-1939.

Almar, R., Castelle, B., Ruessink, B. G., Senechal, N., Bonneton, P., & Marieu, V., 2009. High-frequency video observation of two nearby double-barred beaches under high-energy wave forcing. J Coast Res SI56, 1706–1710.

Angnuureng, D. B., Almar, R., Senechal, N., Castelle, B., Appeaning Addo, K., Marieu, V., & Ranasinghe, R., 2017. Two and three-dimensional shoreline behaviour at a MESO-MACROTIDAL barred beach. Journal of Coastal Conservation, 21(3), 381‑392. https://doi.org/10.1007/s11852-017-0516-6.

Angnuureng, D. B., Almar, R., Senechal, N., Castelle, B., Addo, K. A., Marieu, V., & Ranasinghe, R., 2017. Shoreline resilience to individual storms and storm clusters on a meso-macrotidal barred beach. Geomorphology, 290, 265‑276. https://doi.org/10.1016/j.geomorph.2017.04.007.

Anthony, E. J., 2013. Storms, shoreface morphodynamics, sand supply, and the accretion and erosion of coastal dune barriers in the southern North Sea. Geomorphology.

Ba, A., & Senechal, N., 2013. Extreme winter storm versus Summer storm: morphological impact on a sandy beach. Journal of Coastal Research, 65(sp1), 648-653.

Baart, F., van Ormondt, M., van Thiel de Vries, J. S. M., & van Koningsveld, M., 2015. Morphological impact of a storm can be predicted three days ahead. Computers & Geosciences, 90, 17‑23. https://doi.org/10.1016/j.cageo.2015.11.011.

Battiau-Queney, Y., Billet, J. F., Chaverot, S., & Lanoy-Ratel, P., 2003. Recent shoreline mobility and geomorphologic evolution of macrotidal sandy beaches in the north of France. Marine geology, 194(1-2), 31-45.

Butel, R., Dupuis, H., & Bonneton, P., 2002. Spatial Variability of Wave Conditions on the French Atlantic Coast using In-Situ Data. Journal of Coastal Research, (36), 13.

Biausque, M., Senechal, N., Blossier, B., & Bryan, K. R., 2016. Seasonal Variations in Recovery Timescales of Shorelines on an Embayed Beach. Proceeding of ICS, 2016- Sydney– Australia. Journal of Coastal Research, 75(sp1), 353-357.

Biausque, M., Senechal, N., Barre, A., & Laigre, T., 2017. HIGH FREQUENCY MONITORING OF THE SHORELINE/BARLINE EVOLUTION OF AN OPEN SANDY BEACH, THE EXAMPLE OF BISCARROSSE BEACH (FRANCE). Proceedings of Coastal Dynamics 2017, Danemark, 8.

Biausque, M., & Senechal, N., 2018. Storms impacts on a sandy beach including seasonal recovery: alongshore variability and management influences. Revue Paralia. *Accepted*.

Boak, E. H., & Turner, I. L., 2005. Shoreline Definition and Detection: A Review. Journal of Coastal Research, 214, 688‑703. https://doi.org/10.2112/03-0071.1

Brooks, S.M., Spencer, T., Christie, E.K., 2017. Storm impacts and shoreline recovery: Mechanisms and controls in the southern North Sea. Geomorphology, 283:48-60.

Burvingt, O., Masselink, G., Russell, P., Scott, T., 2017. Classification of Beach Response to Extreme Storms. Geomorphology, 295, 722‑ 37. https://doi.org/10.1016/j.geomorph.2017.07.022.

Castelle, B., Bonneton, P., Dupuis, H., & Sénéchal, N., 2007. Double bar beach dynamics on the high-energy meso-macrotidal French Aquitanian Coast: A review. Marine Geology, 245(1‑4), 141‑159. https://doi.org/10.1016/j.margeo.2007.06.001.

Castelle, B., Marieu, V., Bujan, S., Ferreira, S., Parisot, J.-P., Capo, S., … Chouzenoux, T., 2014. Equilibrium shoreline modelling of a high-energy meso-macrotidal multiple-barred beach. Marine Geology, 347, 85‑94. https://doi.org/10.1016/j.margeo.2013.11.003

Coco, G., Senechal, N., Rejas, A., Bryan, K. R., Capo, S., Parisot, J. P., ... & MacMahan, J. H., 2014. Beach response to a sequence of extreme storms. Geomorphology, 204, 493-501.

Corbella, S., & Stretch, D. D., 2011. Shoreline recovery from storms on the east coast of Southern Africa. Natural Hazards and Earth System Science, 12(1), 11‑22.
https://doi.org/10.5194/nhess-12-11-2012.

Davidson, M. A., Turner, I. L., Splinter, K. D., & Harley, M. D., 2017. Annual prediction of shoreline erosion and subsequent recovery. Coastal Engineering, 130, 14-25.

Dehouck, A., Lafon, V., Senechal, N., Froidefond, J.M., Almar, R., Castelle, B., Martiny, N., 2012. Inter-annual morphodynamic evolution of the South coast of the Gironde. Revue Française de Photogrammetrie et de Teledection, 197:31-42.

Dissanayake, P., Brown, J., & Karunarathna, H., 2015. Impacts of storm chronology on the morphological changes of the Formby beach and dune system, UK. Nat. Hazards Earth Syst. Sci., 15(7), 1533‑1543. https://doi.org/10.5194/nhess-15-1533-2015.

Durgappa, R., 2008. Coastal protection works, Seventh International Conference of Coastal and Port Engineering in Developing Countries, COPEDEC VII, Dubai, 1–15 March 2008, 97.

Dolan, R., & Davis, R. E.,1994. Coastal storm hazards. Journal of Coastal Research, 103‑114.

Feagin, R. A., Sherman, D. J., & Grant, W. E., 2005. Coastal erosion, global sea-level rise, and the loss of sand dune plant habitats. Frontiers in Ecology and the Environment, 3(7), 359-364.

Harley, M. D., Turner, I. L., Kinsela, M. A., Middleton, J. H., Mumford, P. J., Splinter, K. D., ... & Short, A. D., 2017. Extreme coastal erosion enhanced by anomalous extratropical storm wave direction. Scientific reports, 7(1), 6033.

Idier, D., Charles, E., Mallet, C., Castelle, B., 2013. Longshore sediment flux hindcast and potential impact of future climate change along the Gironde/Landes Coast, SW France. Journal of Coastal research, SI65:1785-1790.

Lafon, V., Dupuis, H., Butel, R., Castelle, B., Michel, D., Howa, H., & Apoluceno, D. D. M., 2005. Morphodynamics of nearshore rhythmic sandbars in a mixed-energy environment (SW France): 2. Physical forcing analysis. Estuarine, Coastal and Shelf Science, 65(3), 449-462.

van de Lageweg, W. I., Bryan, K. R., Coco, G., & Ruessink, B. G.,2013. Observations of shoreline–sandbar coupling on an embayed beach. Marine Geology, 344, 101‑114. https://doi.org/10.1016/j.margeo.2013.07.018

Larson, M., & Kraus, N. C., 1989. SBEACH: numerical model for simulating storm-induced beach change. Report 1. Empirical foundation and model development (No. CERC-TR-89-9). Coastal Engineering Research Center Vicksburg Ms.

Lippmann, T., & Holman, R., 1989. Quantification of Sand Bar Morphology: A Video Technique Based on Wave Dissipation. JOURNAL OF GEOPHYSICAL RESEARCH, 94(C1), 995-1011.

Loureiro, C., Ferreira, Ó., Cooper, J.A.G., 2012. Extreme erosion on high-energy embayed beaches: Influence of megarips and storm grouping. Geomorphology, 139–140, 155–171. https://doi.org/10.1016/j.geomorph.2011.10.013

Ludka, B. C., Guza, R. T., O'Reilly, W. C., & Yates, M. L., 2015. Field evidence of beach profile evolution toward equilibrium. Journal of Geophysical Research: Oceans, 120(11), 7574-7597.

Marshall, J., Kushnir, Y., Battisti, D., Chang, P., Czaja, A., Dickson, R., ... & Visbeck, M., 2001. North Atlantic climate variability: phenomena, impacts and mechanisms. International Journal of Climatology, 21(15), 1863-1898.

Masselink, G., & Pattiaratchi, C. B., 2001. Seasonal changes in beach morphology along the sheltered coastline of Perth, Western Australia. Marine Geology, 172(3-4), 243-263.

Masselink, G., Hughes, M., & Knight, J., 2014. Introduction to coastal processes and geomorphology. Routledge.

Masselink, G., & van Heteren, S., 2014. Response of wave-dominated and mixed-energy barriers to storms. Marine Geology, 352, 321‐347. https://doi.org/10.1016/j.margeo.2013.11.004

Masselink, G., Castelle, B., Scott, T., Dodet, G., Suanez, S., Jackson, D., & Floc'h, F., 2016. Extreme wave activity during 2013/2014 winter and morphological impacts along the Atlantic coast of Europe: EXTREME ATLANTIC WAVES DURING 2013/2014. Geophysical Research Letters, 43(5), 2135‐2143. https://doi.org/10.1002/2015GL067492.

Morris, B.D., Davidson, M.A., Huntley, D.A., 2001. Measurements of the response of a coastal inlet using video monitoring techniques. Marine Geology 175, 251–272. https://doi.org/10.1016/S0025-3227(01)00144-X

Pender, D., & Karunarathna, H., 2013. A statistical-process based approach for modelling beach profile variability. Coastal Engineering, 81, 19‐29. https://doi.org/10.1016/j.coastaleng.2013.06.006.

Péron, C., & Sénéchal, N., 2011. Dynamic of a meso to macro-tidal double barred beach: inner bar response. Journal of Coastal Research, (64), 120.

Phillips, M. S., Harley, M. D., Turner, I. L., Splinter, K. D., & Cox, R. J., 2017. Shoreline recovery on wave-dominated sandy coastlines: the role of sandbar morphodynamics and nearshore wave parameters. Marine Geology, 385, 146-159.

Reeve, D. E., Karunarathna, H., Pan, S., Horrillo-Caraballo, J. M., Różyński, G., & Ranasinghe, R., 2016. Data-driven and hybrid coastal morphological prediction methods for mesoscale forecasting. Geomorphology, 256, 49‐67. https://doi.org/10.1016/j.geomorph.2015.10.016.

van Rijn, L. C., 2014. A simple general expression for longshore transport of sand, gravel and shingle. Coastal Engineering, 90, 23-39.

Scott, T., Masselink, G., O'Hare, T., Saulter, A., Poate, T., Russell, P., … Conley, D., 2016. The extreme 2013/2014 winter storms: Beach recovery along the southwest coast of England. Marine Geology, 382, 224‐241. https://doi.org/10.1016/j.margeo.2016.10.011.

Senechal, N., Gouriou, T., Castelle, B., Parisot, J.P., Capo, S., Bujan, S. Howa, H., 2009. Morphodynamic response of a meso- macro-tidal intermediate beach based on a long-term data-set, Geomorphology, 107, 263-274.

Senechal, N., Coco, G., Castelle, B., & Marieu, V., 2015. Storm impact on the seasonal shoreline dynamics of a meso-to macrotidal open sandy beach (Biscarrosse, France). Geomorphology, 228, 448-461.

Senechal, N., Castelle, B., Bryan, K. R., 2017. Storm clustering and beach response. In: Coastal Storms: Processes and Impacts edited by Ciavolo, P. & Coco, G., John Wiley & Sons Ltd.

Smith, R. K., & Bryan, K. R., 2007. Monitoring beach face volume with a combination of intermittent profiling and video imagery. Journal of Coastal Research, 892-898.

Splinter, K. D., Turner, I. L., & Davidson, M. A., 2013. How much data is enough? The importance of morphological sampling interval and duration for calibration of empirical shoreline models. Coastal Engineering, 77, 14-27.

Splinter, K. D., Kearney, E. T., & Turner, I. L., 2018. Drivers of alongshore variable dune erosion during a storm event: Observations and modelling. Coastal Engineering, 131, 31 - 41. https://doi.org/10.1016/j.coastaleng.2017.10.011.

Stive, M.J., Aarninkhof, S.G., Hamm, L., Hanson, H., Larson, M., Wijnberg, K.M., Nicholls, R.J., and Capobianco, M., 2002. Variability of shore and shoreline evolution. Coastal Engineering 47, 211–235.

Stive, M. J. F., de Schipper, M. A., Luijendijk, A. P., Aarninkhof, S. G. J., van Gelder-Maas, C., van Thiel de Vries, J. S. M., de Vries, S., Henriquez, M., Marx, S., Ranasinghe, R., 2013. A New Alternative to Saving Our Beaches from Sea-Level Rise: The Sand Engine. Journal of Coastal Research, 1001‑1008. https://doi.org/10.2112/JCOASTRES-D-13-00070.1.

Vousdoukas, M. I., Ferreira, P. M., Almeida, L. P., Dodet, G., Psaros, F., Andriolo, U., … Ferreira, Ó. M., 2011. Performance of intertidal topography video monitoring of a meso-tidal reflective beach in South Portugal. Ocean Dynamics, 61(10), 1521‑1540. https://doi.org/10.1007/s10236-011-0440-5.

Vousdoukas, M.I., Almeida, L.P.M., Ferreira, O., 2012. Beach erosion and recovery during consecutive storms at a steep-sloping, meso-tidal beach. Earth Surface Processes and Landforms, 37:583-593.

Wright, L. D., & Short, A. D., 1984. Morphodynamic variability of surf zones and beaches: a synthesis. Marine geology, 56(1-4), 93-118.

Yates, M. L., Guza, R. T., & O'Reilly, W. C., 2009. Equilibrium shoreline response: Observations and modeling. Journal of Geophysical Research: Oceans, 114(C9).

Highlights

- Similar seasonal sediment budget observed under very contrasting seasonal cumulative wave energy
- Post-storm initiated recovery of the beach not automatically interrupted by the following high energetic conditions due to a storm
- Inter-storm wave conditions play a crucial role in the winter seasonal response of the beach